

On the Nonlinear Shaping Gain with Probabilistic Shaping and Carrier Phase Recovery

Stella Civelli, *Member, IEEE*, Emanuele Parente, Enrico Forestieri, *Senior Member, IEEE*, and Marco Secondini, *Senior Member, IEEE*

Abstract—The performance of different probabilistic amplitude shaping (PAS) techniques in the nonlinear regime is investigated, highlighting its dependence on the PAS block length and the interaction with carrier phase recovery. Different PAS implementations are considered, based on different distribution matching (DM) techniques—namely, sphere shaping, shell mapping with different number of shells, and constant composition DM—and amplitude-to-symbol maps. When carrier phase recovery is not included, PAS with optimal block length provides a nonlinear shaping gain with respect to a linearly optimized PAS (with infinite block length); among the considered DM techniques, the largest gain is obtained with sphere shaping. On the other hand, the nonlinear shaping gain becomes smaller, or completely vanishes, when carrier phase recovery is included, meaning that in this case all the considered implementations achieve a similar performance for a sufficiently long block length. Similar results are obtained in different link configurations (1×180 km, 15×80 km, and 27×80 km single-mode-fiber links), and also including laser phase noise, except when in-line dispersion compensation is used. Furthermore, we define a new metric, the nonlinear phase noise (NPN) metric, which is based on the frequency resolved logarithmic perturbation model and explains the interaction of carrier phase recovery and PAS. We show that the NPN metric is highly correlated with the performance of the system. Our results suggest that, in general, the optimization of PAS in the nonlinear regime should always account for the presence of a carrier phase recovery algorithm. In this case, the reduction of the rate loss (obtained by using sphere shaping and increasing the DM block length) turns out to be more important than the mitigation of the nonlinear phase noise (obtained by using constant-energy DMs and reducing the block length), the latter being already granted by the carrier phase recovery algorithm.

Index Terms—Optical fiber communication, nonlinear fiber channel, probabilistic shaping, phase noise.

I. INTRODUCTION

PROBABILISTIC amplitude shaping (PAS) has been recently widely investigated as a way to improve the performance of an optical fiber network. PAS allows to finely adapt the information rate to the system requirements (channel signal-to-noise ratio (SNR) and forward error correction (FEC) code) and to reduce the gap to the Shannon limit in the linear regime [2]–[4]. The SNR gain—up to 1.53 dB for large constellation size [5]—depends on the particular

implementation of PAS, handled by the distribution matcher (DM). The DM maps k independent input bits with uniform distribution to N output amplitudes with the desired Maxwell–Boltzmann (MB) distribution—the optimal one in the linear regime. To do so, the DM imposes some specific constraints (e.g., a constant composition or a maximum energy) on the N symbols of each block, which are therefore *correlated*. While a DM can be implemented in different ways, its performance generally improves with the block length N . In fact, the correlation between the symbols of each block decreases when N increases, allowing to encode more information per transmitted symbol. For $N \rightarrow \infty$, the correlation vanishes and the DM output looks like an i.i.d. source with MB distribution, yielding the optimal PAS gain in the linear regime for a given rate and constellation size [5].

Previous studies on PAS concerned the DM implementation and PAS performance in the linear regime, aiming at reducing the rate loss—a useful performance metric defined as the difference between the entropy of the target MB distribution and the actual DM rate k/N —with reasonable computational complexity, hardware requirements, and flexibility [3]. For instance, sphere shaping (SS), implemented through the enumerative sphere shaping (ESS) algorithm, provides the best performance for a given block length [6]–[8]; constant composition DM (CCDM), implemented by arithmetic coding, is a simple and flexible technique to obtain the desired target distribution [9], [10]; hierarchical DM (Hi-DM) is an effective approach to combine several short DMs (based, e.g., on simple look-up tables) to form a long DM with good performance and low complexity [11]–[14]. In general, it was shown that increasing the block length N of the DM reduces the rate loss and improves the performance in the linear regime, without any downside (but for the increased latency and difficulties in the DM implementation). The interaction of carrier phase recovery algorithms and PAS was investigated in [15], considering the ideal MB distribution in the linear regime.

More recently, the performance of PAS in the nonlinear regime has been studied [4], and it was shown, firstly for SS [16] and later for CCDM [17], that increasing the block length at will is not beneficial. Indeed, the constraints induced by the DM on the N symbols of each block, besides reducing the rate of the source causing a rate loss, usually reduce also the intensity fluctuations on the signal, hence reducing the amount of nonlinear interference generated by each channel and yielding an additional *nonlinear shaping gain*. In this case, the correlation induced by the DM is beneficial, so that the nonlinear shaping gain decreases as N increases,

S. Civelli, E. Forestieri, and M. Secondini are with the Institute of Communication, Information and Perception Technologies, Scuola Superiore Sant’Anna, Pisa, Italy, and with the National Laboratory of Photonic Networks, CNIT, Pisa, Italy. E. Parente is with the Institute of Communication, Information and Perception Technologies, Scuola Superiore Sant’Anna, Pisa, Italy. Email: stella.civelli@santannapisa.it.

This paper was presented in part at the European Conference on Optical Communication (ECOC), Bruxelles, Belgium, December 6-10, 2020 [1].

vanishing for $N \rightarrow \infty$. Therefore, there is an optimal block length that maximizes the shaping gain by providing the best trade-off between linear and nonlinear gain. The nonlinear interference due to DM was analyzed in [18] for the CCDM, while the kurtosis-limited sphere shaping, which selects the sequences with minimum energy and low kurtosis, showed superior performance in the nonlinear regime with respect to equivalent-length ESS in a single-span scenario but not for a multi-span link [19]. Furthermore, it was shown that the nonlinear shaping gain improves by properly packing shaped sequences in time and frequency [20].

However, it is also known that a good part of the inter-channel nonlinear interference generated by intensity fluctuations (which are reduced by a short-block-length DM, as explained above) manifests as correlated phase noise, which can be mitigated also by a properly optimized carrier phase recovery algorithm [21]–[25]. Unfortunately, a preliminary study on the interaction between the nonlinear shaping gain and carrier phase recovery algorithms showed that the gain provided by the two techniques is very similar and does not add up [1]. Similar conclusions were drawn by an analytical study about the interaction of carrier phase recovery and CCDM for cross phase modulation [26]. This effect is particularly relevant from a system design perspective, since a carrier recovery algorithm is always included in practical systems, meaning that the nonlinear shaping gain observed in simulations in the absence of a carrier recovery algorithm, might in fact disappear (or be drastically reduced) in realistic systems. In this work, we extend the analysis in [1] to assess the interaction between carrier phase recovery and PAS in terms of nonlinearity mitigation in a wavelength-division multiplexing (WDM) scenario. This is done by including the laser phase noise in the system, highlighting the performance of different PAS and DM implementations, considering different scenarios, and introducing a new performance metric to study and predict this interaction.

II. PROBABILISTIC AMPLITUDE SHAPING

PAS is implemented at the transmitter by using four identical DMs. Each DM maps k uniformly distributed bits to N shaped amplitudes, A_1, \dots, A_N . The $4N$ amplitudes are then combined with $4N$ signs (obtained from other $4N$ uniform bits) and mapped to the four components of N dual-polarization QAM symbols (i.e., 4D symbols).¹ The amplitude-to-symbol mapping can be done in several ways. Here, we consider the two maps sketched in Fig. 1, referred to as *serial map* and *parallel map*. On the one hand, the serial map maps the N amplitudes generated by the first DM to the four components of the first $N/4$ 4D symbols, the N amplitudes generated by the second DM to the four components of the subsequent $N/4$ 4D symbols, and so on. On the other hand, the parallel map maps the N amplitudes of the first DM to the first component of the N 4D symbols, the N amplitudes of the second DM to the second component of the N 4D symbols, and so on. While the serial map induces

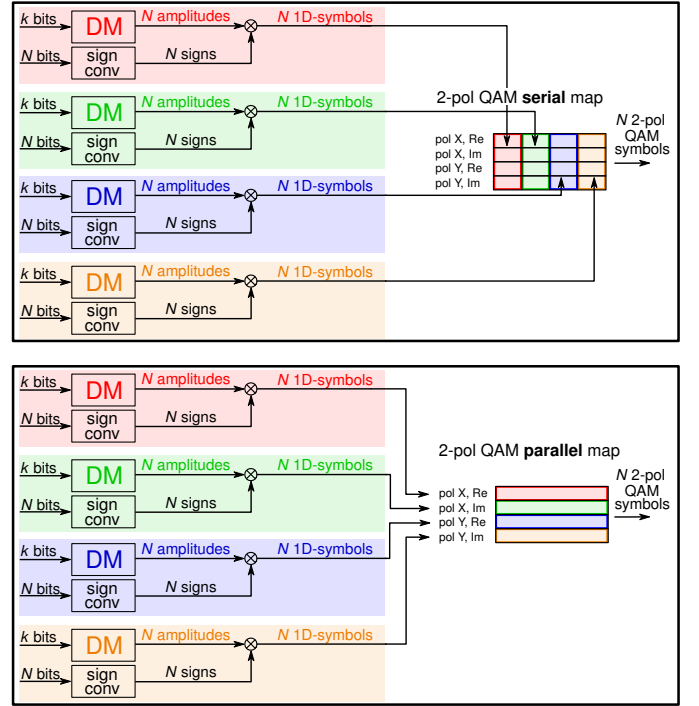


Figure 1. Different mappings to generate N 2-pol QAM symbols from $4N$ amplitudes generated by four instances of the same DM and $4N$ i.i.d. bits used for the signs.

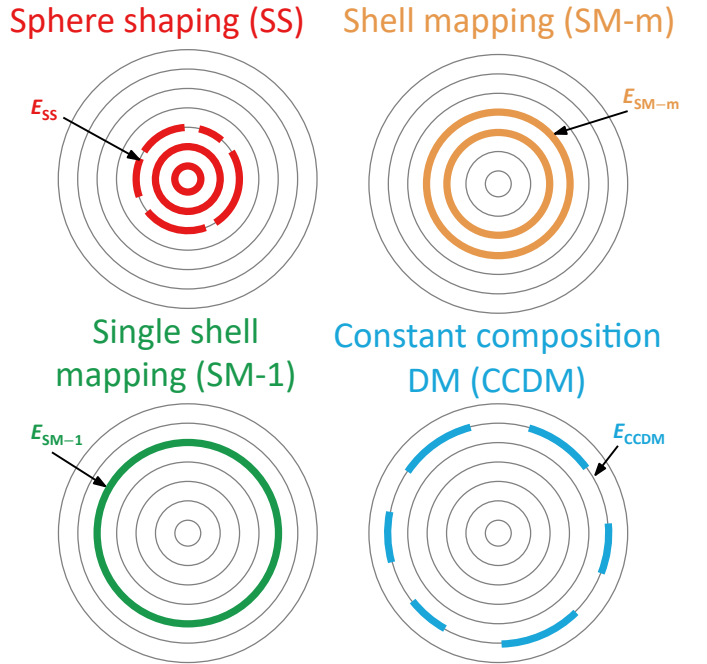


Figure 2. 2-dimensional energy description of different DM techniques. Black thin circles represent possible energy levels.

¹The reverse concatenation with the FEC is irrelevant to this description and is therefore omitted.

a stronger correlation (the four components are correlated) on a shorter block of $N/4$ adjacent symbols, the parallel map induces a weaker correlation (the four components are independent) on a longer block of N adjacent symbols. The two maps are equivalent in the linear regime but, as we will see in the following, they provide different performance in the nonlinear regime.

For the PAS implementation, we consider different DM techniques: SS, shell mapping (SM), and CCDDM, as described below. The energy distribution of the methods is qualitatively depicted in Fig. 2.

SS maps k bits to the 2^k lowest-energy sequences of N amplitudes. Thus, by representing each sequence as a point in an N -dimensional space, all the sequences must lie within the smallest possible sphere that contains at least 2^k sequences. The map covers all the sequences *inside* the sphere and some of the sequences *on* the sphere, as shown qualitatively in Fig. 2. The average energy of the sequences is E_{SS} . SS is implemented using the ESS algorithm [6], [27], [28], resorting to the double-trellis trick proposed in [13] and studied in [29] to obtain optimal performance. For a given block length N and constellation size, SS maximizes the source rate for a given average energy, yielding the best performance in the linear regime.

SM maps k bits to the 2^k lowest-energy sequences, with the additional constraint that at most m energy levels (shells) can be occupied—indicated as SM- m . Thus, SM-1 uses only sequences that lie in a single shell and, therefore, have the same energy; SM-2 uses two adjacent shells; and so on. When the number of shells increases, SM- m tends to SS. The energy of the sequences covered by SM- m is limited by a maximum and a minimum value, with E_{SM-m} being the average energy. Also SM is implemented by using the ESS algorithm; the recently proposed band-ESS can also be used [30]. In the following, we consider only two extreme cases: the single-shell case, denoted as SM-1, and the case with the maximum number of shells (but lower than SS), denoted as SM-max. The latter is obtained by adding one higher-energy shell to those used by SS and removing all the innermost ones that are no longer needed (the number of shells m varies in this case).

CCDDM maps k bits on 2^k amplitude sequences with the same composition, i.e., permutations of the same sequence [9], [31]. The composition is determined by the desired target distribution. Since the sequences have the same composition, they also have the same energy E_{CCDDM} and lie in a single shell, as in the SM-1 case.

In the linear regime, for a given block length N and constellation size, the PAS performance depends on the average energy E_{DM} of the 2^k sequences used by the considered DM. It is simple to verify that $E_{CCDDM} \geq E_{SM-1} \geq E_{SM-2} \geq \dots \geq E_{SM-max} \geq E_{SS}$. Thus, the best performance is obtained with SS, then with SM- m (the performance decreasing with decreasing m), and eventually with CCDDM. As the block length N increases, all the mentioned methods approach an i.i.d. source with MB distribution [5], which yields the ultimate linear shaping gain (and zero rate and energy losses).

On the other hand, in the nonlinear regime, the capacity-

achieving distribution and, consequently, the optimal DM are unknown. However, some useful design guidelines can be obtained from approximate models or observations. For instance, it has been shown that the amount of nonlinear interference generated by a propagating signal depends not only on its average power (second-order moment), but also on its fourth-order moment (when symbols are i.i.d.) [22], [32]–[34] or, more in general, on the variations of the instantaneous power over a finite temporal window [18], [20], [35]. In this case, the use of a shorter block length N is expected to be beneficial, as it introduces a constraint on the energy of each block of N symbols. The constraint is stronger for CCDDM and SM-1 (for which the energy of each sequence is constant), and becomes weaker for SM- m as m increases (since the energy of each sequence may take m different values). Therefore, as opposed to the ranking defined in terms of linear performance, we expect CCDDM and SM-1 to provide the most effective nonlinearity mitigation, followed by SM-2, SM-3, and so on, while SS should be the least effective. As a result, the optimization of both the DM type and its block length should aim to obtain the best trade-off between two conflicting objectives: the reduction of the rate loss (linear shaping gain) and the reduction of the intensity fluctuations (nonlinear shaping gain). This will be investigated in Section VI.

To study the behavior of different DMs as a function of the block length N , we resort to a trick to emulate SS and SM- m for $N > 512$, when the rate loss of the two methods is very small, but the computation of the required trellis structures becomes nearly unfeasible. In this case, we concatenate the amplitudes generated by $N/512$ independent uses of a DM of block length 512, followed by an interleaver of length N . In this manner, we emulate the correlation induced by a DM of block length N , while achieving almost the same rate loss.

III. NONLINEAR PHASE NOISE METRIC

Different fiber nonlinearity models agree that a relevant portion of nonlinear interference—in particular that generated by the intensity fluctuations of the signal—manifests as phase noise [21], [22], [32], [33]. For instance, the frequency-resolved logarithmic perturbation (FRLP) model describes nonlinear interference as a frequency-dependent phase noise that can be expressed as a quadratic form of the symbols transmitted in a certain time window around the considered time on the (self- or cross-) interfering channels [33], [36].² For i.i.d. symbols, the variance of this phase noise depends on the kurtosis of the symbols, so that non-constant-envelope modulations (e.g., QAM or Gaussian modulation) cause a stronger NLI than constant-envelope modulations (e.g., PSK) [33]. However, the nonlinear phase noise generated by non-constant-envelope modulations is strongly correlated in time, so that it can be mitigated by a suitable carrier-phase recovery algorithm, after which its variance practically reduces to that of constant-envelope modulation [37]. Here, we extend the

²Though the window formally extend over an infinite time, the coefficients of the quadratic form rapidly decays outside a finite time window determined by the walk-off time between the frequency components involved in the interference process.

analysis to the case of correlated symbols, such as those generated by the PAS schemes described in Section II, with the aim of finding a suitable metric to predict the dependence of the generated NLI on the PAS block length, accounting for the possible presence of a carrier-phase recovery algorithm. With respect to [33], since removing the i.i.d. assumption significantly complicates the analysis [38], we further simplify the FRLP model to obtain a nonlinear phase noise model that depends only on signal intensity, and resort to a numerical approach for the computation of the variance.

The simplified nonlinear phase noise model is derived from the FRLP model [33] by following the same approach used in [39]–[42] to develop the enhanced split-step Fourier method (ESSFM) and the coupled-channel ESSFM (CESSFM) algorithms for DBP. By considering only the terms on the diagonal of the quadratic form in [33, eq. (18)], neglecting (or averaging out) their dependence on frequency, and accounting for the contributions of the two polarizations of each interfering channel, we eventually obtain a simple phase noise term that depends on the intensity variations of all the interfering channels. Specifically, considering M WDM channels, denoting by $x_i[k]$ and $y_i[k]$ the normalized k th symbols transmitted on the two polarizations of the i th channel, the corresponding output samples after dispersion compensation can be expressed as $x_i[k] \exp(-j\theta_i[k])$ and $y_i[k] \exp(-j\theta_i[k])$, where

$$\theta_i[k] = \sum_{\ell=1}^M \bar{\phi}_{i\ell} \sum_{m=-N_c}^{N_c} C_{\ell-i}[m] (|x_\ell[k+m]|^2 + |y_\ell[k+m]|^2) \quad (1)$$

is the overall nonlinear phase rotation [42]. In (1), $C_{\ell-i}[m]$ ($m = -N_c, \dots, N_c$) are $2N_c + 1$ real coefficients accounting for the interaction of dispersion and nonlinearity induced by channel ℓ over channel i ; $\bar{\phi}_{i\ell} = (3/2 - \delta_{i\ell}/2)\gamma \int_0^L P_\ell(\zeta) d\zeta$ is the average nonlinear phase rotation induced by channel ℓ over channel i , with $P_\ell(\zeta)$ the power of channel ℓ at distance ζ , L the length of the link, γ the nonlinear coefficient of the fiber, and $\delta_{i\ell}$ the Kronecker delta. The coefficients can be evaluated analytically from [33, eq. (19)]³

$$C_n[m] = T^2 \int_{\frac{2n-1}{2T}}^{\frac{2n+1}{2T}} \int_{\frac{2n-1}{2T}}^{\frac{2n+1}{2T}} K(\mu, \nu) e^{-j2\pi(\mu-\nu)mT} d\mu d\nu \quad (2)$$

where T is the symbol time and $K(\mu, \nu)$ is a function that depends on the link characteristics and accounts for the nonlinear interaction efficiency of different frequency components. Considering a dispersion-unmanaged link made of N_s identical fiber spans of length L_s , with attenuation coefficient α , dispersion parameter β_2 , nonlinear coefficient γ , and ideal dispersion compensation at the end of the link, we have

$$K(\mu, \nu) = \frac{\exp[-\alpha + j4\pi^2\beta_2\nu(\nu - \mu)L_s] - 1}{-\alpha + j4\pi^2\beta_2\nu(\nu - \mu)} \times \frac{\exp[j4\pi^2\beta_2\nu(\nu - \mu)N_sL_s] - 1}{\exp[j4\pi^2\beta_2\nu(\nu - \mu)L_s] - 1} \frac{\alpha}{N_s(1 - e^{-\alpha L_s})} \quad (3)$$

³In this case, we consider only the diagonal terms of the quadratic form, neglect their dependence on frequency, assume an ideal sinc pulse shape, and adopt a different normalization

Interestingly, there is a clear similarity between the nonlinear phase rotation in (1) and the weighted sum of symbol energies used in [18], [35] to define the energy dispersion index (EDI) and the exponentially-weighted EDI (EEDI) and predict the nonlinear shaping gain that occurs in a PAS system using CCDM. For example, the EEDI is defined as [35]

$$\text{EEDI} = \frac{\text{Var}(G^\lambda[k])}{E(G^\lambda[k])} \quad (4)$$

where $E(\cdot)$ denotes expectation,

$$G^\lambda[k] = \sum_{m=-\infty}^{+\infty} \lambda^{|m|} |x_i[k+m]|^2 \quad (5)$$

and $0 \leq \lambda \leq 1$ is a forgetting factor.⁴ This similarity provides a physical explanation of why EDI and EEDI are good predictors of the nonlinear shaping gain (when they are small, the signal is affected by less nonlinear phase noise). The main difference between (5) and (1) is that the coefficients in (1) depend on the link characteristics and can be obtained analytically, while the parameter λ in (5) (or the window length W in the EDI) is optimized a posteriori, through extensive simulations, to maximize the correlation with the system performance. Moreover, (1) accounts for both polarizations and includes the interfering channels. Therefore, we propose to replace the EDI or EEDI with the variance of (1) as a predictor of the nonlinear shaping gain of PAS systems. This solution avoids the use of extensive simulations, poses performance prediction on a more physical ground—relating it to the amount of nonlinear phase noise accumulated during propagation—and, as shown below, allows to easily account for the impact of carrier phase recovery.

In order to account for the randomness of the carrier phase and its temporal variations due to laser phase noise, coherent optical receivers usually include a carrier phase recovery algorithm. Practical algorithms, though not specifically designed for this purpose, can partly mitigate also the nonlinear phase noise in (1), reducing its variance. Of course, the amount of nonlinearity that can be mitigated depends on the specific algorithm and on the width of the time window over which the carrier phase is estimated (or any other parameter playing an analogous role). As with the conventional phase noise due to lasers, a longer time window allows to average out more effectively the impact of additive white Gaussian noise on the estimate, but reduces the ability to track fast changes of the phase.

The above considerations have two important consequences. First, when estimating the effectiveness of PAS as a nonlinear mitigation strategy, the presence of carrier phase recovery should be accounted for. Second, the optimization of the PAS block length N and of the carrier phase recovery block length N_{CPR} are intertwined: they depend on each other and should be done jointly, accounting for the link configuration, the signal-to-noise ratio, and the laser linewidth.

⁴A similar definition holds for the EDI, with the only difference of considering a finite sum of W elements with $\lambda = 1$.

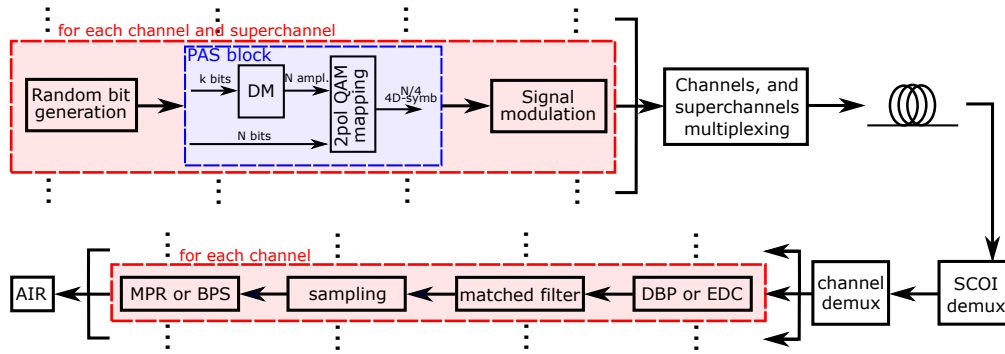


Figure 3. System setup

With this in mind we define the nonlinear phase noise (NPN) metric (for the generic i th channel) as

$$\sigma_{\theta}^2 = \text{Var}(\theta_i[k] - \hat{\theta}_i[k]) + \sigma_{\xi}^2 \quad (6)$$

where

$$\hat{\theta}_i[k] = \frac{\sum_{m=-N_{\text{CPR}}}^{N_{\text{CPR}}} \theta_i[m+k]}{2N_{\text{CPR}} + 1}. \quad (7)$$

is the noiseless estimate of the nonlinear phase rotation at time k provided by the CPR, which we assume to equal the average nonlinear phase noise measured over a window of $2N_{\text{CPR}} + 1$ symbols around the k th symbol, and σ_{ξ}^2 is the variance of the noise affecting the CPR estimate. In general, the latter depends on the specific CPR algorithm, on its block length (or other equivalent parameter), and on the signal-to-noise ratio (SNR). Here, for the sake of simplicity, we assume

$$\sigma_{\xi}^2 = \frac{(2E_s/N_0)^{-1}/(2N_{\text{CPR}} + 1)}{e_{\text{CPR}}} \quad (8)$$

where the numerator is the Cramér-Rao lower bound, and $e_{\text{CPR}} \leq 1$ is a coefficient that measures the efficiency of the CPR algorithm with respect to the bound [43]. In principle, different definitions of (7) and (8) could be employed to account more precisely for the actual behaviour of a specific CPR algorithm, though this is outside the scope of this work.

IV. SIMULATION SETUP

The system setup is sketched in Fig. 3, and is the same considered in [1]. A stream of uniformly distributed bits—representing the information bits after FEC encoding—feeds the PAS block (see Section II), which maps the bits to symbols of a dual polarization 256-QAM constellation with rate 6 bits/symbol/pol. Using a root raised cosine (RRC) pulse with rolloff 0.1 and baud rate $R_s = 41.67$ GBd, the signals corresponding to 4 adjacent channels are multiplexed in a single superchannel, the superchannel of interest (SCOI), with 75 GHz spacing. Two additional superchannels, with the same properties of the SCOI, are also multiplexed, such that 12 evenly spaced channels are transmitted over an overall bandwidth of 900 GHz. The generated WDM waveform is launched into the link, composed of several spans of 80 km single mode fiber (SMF) with dispersion $D = 17$ ps/nm/km, Kerr parameter $\gamma = 1.3 \text{ W}^{-1}\text{km}^{-1}$, and attenuation $\alpha_{\text{dB}} = 0.2$ dB/km. After each span, an erbium-doped fiber amplifier

(EDFA) with noise figure 5 dB compensates for loss. At the end of the link, the side superchannels are filtered out, and the 4 channels of the SCOI are demultiplexed. The transmitter and receiver laser linewidth $\Delta\nu$ are set to either 0 or 100 kHz. Each channel undergoes: (i) either ideal digital back propagation (DBP) or electronic dispersion compensation (EDC), (ii) matched filtering, (iii) sampling at symbol time, and (iv) carrier phase recovery. Finally, the average achievable information rate (AIR) of the 4 channels of the SCOI is evaluated, representing the average information per symbol that can be reliably transmitted on each polarization and channel of the SCOI, assuming an ideal FEC and bit-wise mismatched decoding optimized for the AWGN channel [10], [44], [45].

As regards the carrier phase recovery, two different approaches are considered: mean phase rotation (MPR) and blind phase search (BPS). On the one hand, MPR is the typical approach employed in simulations—when the laser phase noise is not considered and, thus, carrier phase recovery not required—to remove the (constant in time) expected value of the nonlinear phase rotation induced by fiber nonlinearity for a given total launch power. In practice, the MPR is estimated by a simple data-aided procedure—i.e., by averaging the instantaneous phase rotation experienced by all the transmitted symbols after propagation—and then removed from all the received symbols. On the other hand, BPS is a practical carrier phase recovery algorithm typically employed with QAM constellations to track the random fluctuations of the carrier phase induced by laser phase noise [43]. In a nutshell, BPS estimates the carrier phase at discrete time k as the phase rotation (selected among a certain number of test phases) that minimizes the mean square error between the rotated symbols and the corresponding QAM decisions over a window of $2N_{\text{CPR}} + 1$ symbols centered at time k . A shorter window can track faster phase variations, whereas a longer window is required to average out the impact of ASE noise more effectively. The optimal window width is the trade-off between these two effects. In the following, we optimize N_{CPR} numerically and consider 64 test phases in a $\pi/2$ interval. The MPR is nearly equivalent to a BPS with $N_{\text{CPR}} \rightarrow \infty$.

The phase estimated by BPS is affected by an ambiguity of multiples of $\pi/2$ due to the 4-fold rotational symmetry of conventional QAM constellations. This ambiguity may induce

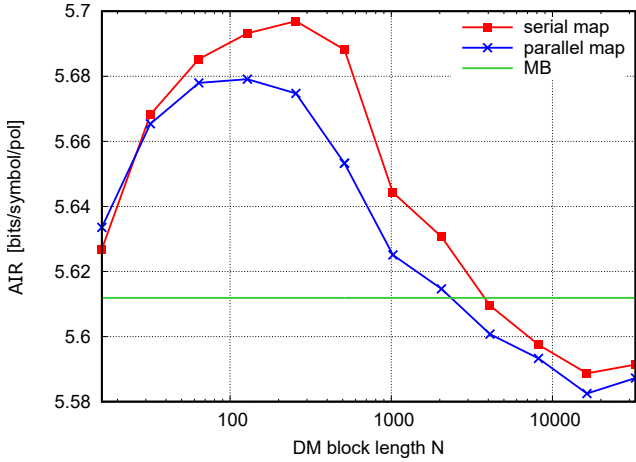


Figure 4. AIR versus block length for different strategies to map amplitudes to symbols. 15×80 km link, EDC, no BPS.

detrimental cycle slips, but can be avoided by using, for example, differential coding or pilot symbols [43]. In our simulations, for the sake of simplicity, when laser phase noise is included in the system, we further apply a supervised cycle-slip compensation after BPS [15].

V. NUMERICAL RESULTS

First, we investigate the performance of the different PAS and bit-to-amplitude mapping schemes presented in Section II. Figure 4 compares the performance of the serial and parallel bit-to-amplitude maps at the optimal launch power ($P = 6$ dBm per superchannel) for different block lengths. In this case, PAS is implemented with the ESS algorithm, DBP is not applied, the laser linewidth is set to zero, and the BPS carrier-recovery algorithm is not employed. As a reference, the performance obtained with MB-distributed i.i.d. symbols (optimal in the linear regime) is also shown. When the block length is very short, up to $N \approx 32$, the two maps perform the same, since the performance is limited by the large rate loss. For longer block lengths, the serial map performs better than the parallel one and achieves the highest AIR, with a gain of approximately 0.02 bits/symbol/pol over the parallel map—a similar behaviour was shown in [46], [47] for a single polarization QAM map. The superiority of the serial map is explained by the fact that, for a given DM block length, it constraints the signal energy on a four-time shorter time interval (twice shorter in the single-polarization case) compared to the parallel map, reducing the intensity fluctuations and the corresponding nonlinear phase noise. Both curves improve up to an optimal point ($N \approx 256$ and $N \approx 128$ for the serial map and for the parallel map, respectively) and decrease afterwards to approach the MB curve for $N \rightarrow +\infty$. The peaky behaviour of both curves and the presence of a nonlinear shaping gain compared to the MB reference curve are analyzed in detail in the following, where only the serial map is considered, due to its superior performance.

The performance of different DM are compared in Figs. 5(a)-(b) as a function of the DM block length and with (solid

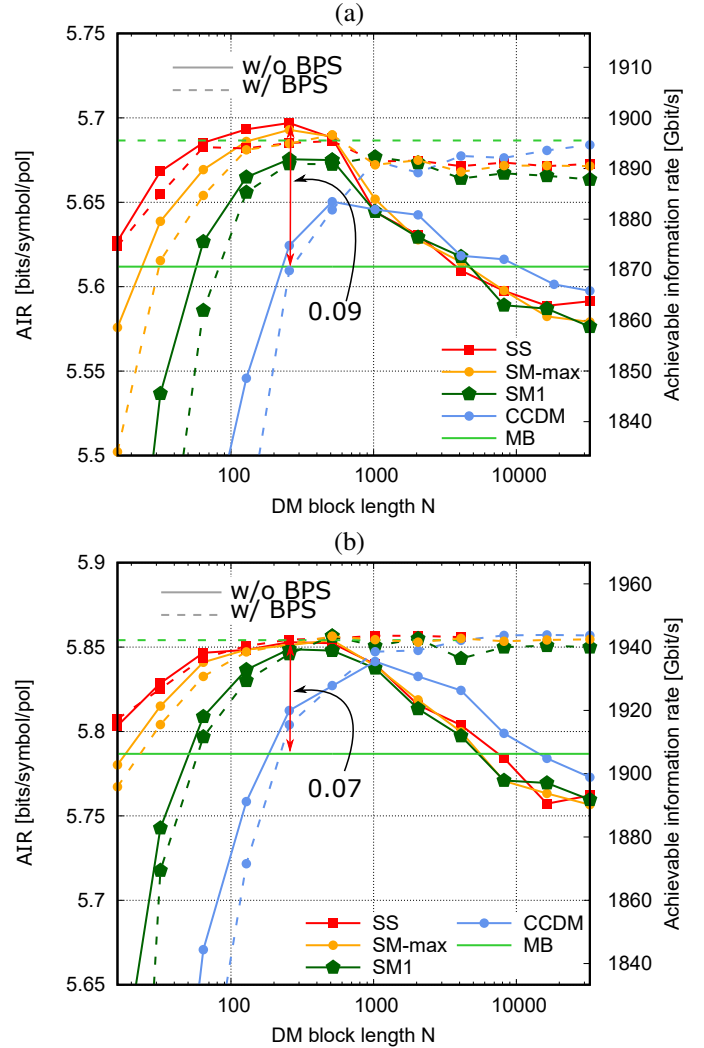


Figure 5. Maximum AIR versus DM block length for 15×80 km link with different DM techniques and with and without BPS (a) EDC with $N_{\text{CPR}} = 24$, and (b) DBP with $N_{\text{CPR}} = 16$.

lines) or without BPS (dashed lines), for the case without DBP in (a) and when ideal DBP is included in (b).

On the one hand, Fig. 5(a) shows that, when BPS is not employed, the performance improves up to a certain optimal point and then decreases, approaching the value obtained with the MB distribution—indicating the value obtained with a DM with infinite block length. The difference between the optimal performance and the MB line is the nonlinear shaping gain [4], [16], [17]. This happens because while as the block length increases the rate loss decreases and the linear performance improves, at the same time, the correlations between symbols induced by the DM becomes weaker, diminishing their impact on nonlinearities and deteriorating the performance in the nonlinear regime. The optimal block length is the trade-off between linear performance (rate loss) and nonlinear shaping gain (correlations induced by DM). This behavior happens for all considered DMs, and both with or without DBP. However, the nonlinear shaping gain is the largest for the SS (approximately equal to 0.085 bit/symbol/pol), just slightly smaller for SM, smaller for SM1, and the smallest for CCDM,

following the same ranking shown in the linear regime. Since SM reduces the intensity fluctuations of the signal with respect to SS, one could expect the SM or the SM1 to provide the best nonlinear performance—as shown in [30] for a 205km fiber—, the SS (and then in order SM, SM1 and CCDM) has the smaller rate loss, thus allowing to consider shorter block lengths where the correlations are stronger. The nonlinear behavior of the CCDM can be predicted using the energy dispersion index [18], [35]. The superior performance of SS with respect to CCDM in the nonlinear regime was also shown in [48] and experimentally in [49].

On the other hand, Fig. 5(a) shows that when BPS is employed, the performance of all methods improves almost monotonically towards the MB curve, without any loss. There is not a nonlinear shaping gain in this case, meaning that the BPS is mitigating the same inter-channel nonlinearities mitigated by short block length PAS. When the BPS is employed, the optimal performance can be obtained by using PAS with a sufficiently high block length to reduce the rate loss, without a specific block length optimization. The performance for short block lengths follows the same ranking given in the linear regime, as for the case without BPS. For short block lengths, the performance of the curves with BPS are slightly worse than those with BPS—this happens because the BPS has been optimized for the MB curve, which has a larger SNR.

Fig. 5(b) shows the same as Fig. 5(a), but adding ideal DBP. The performance improves, since DBP is applied, but the overall behavior does not change with respect to Fig. 5(a). This result confirms that DBP and PAS (or DBP and BPS) mitigate different nonlinearities—intra- and inter-channel, respectively—and that their gains add up. When BPS is not employed, besides some interesting results on the nonlinear shaping gain, the most important finding revealed by Figs. 5(a)-(b) is that the nonlinear shaping gain is not relevant when the BPS is employed and optimized to minimize nonlinearities. However, while a carrier phase recovery algorithm is always included in a system, its block length depends on the laser phase noise of the TX and RX laser, which may change the overall behavior. Its impact is investigated in Figs. 6(a)-(b), which show the AIR versus DM block length for a (a) 15×80 km and (b) 27×80 km link, when a laser with linewidth $\Delta\nu = 100$ kHz is considered at the TX and RX sides. The block length of the BPS—optimized to mitigate the laser phase noise for the MB case when DBP is not applied—is $N_{\text{CPR}} = 38$ and $N_{\text{CPR}} = 94$ in (a) and (b), respectively. In the 15 spans case, we do not observe any nonlinear shaping gain, while for the 27 span case a small nonlinear shaping gain of approximately 0.05 bit/symbol/pol can be observed. A similar behavior—with a larger gain of ≈ 0.1 bit/symbol/pol—was shown in [1], where the laser phase noise was not included.

Next, the system performance is evaluated for a link made of a single span of SMF of length 180 km, using the SS technique, EDC at the RX, and including the BPS with $N_{\text{CPR}} = 60$ to compensate for the laser phase noise. Fig. 7(a) reports the AIR versus DM block length and shows that the system performance achieves a maximum for $N = 32$ —much shorter than in previous cases—but with a negligible gain (approximately 0.05 bit/symbol/pol) with respect to the ideal

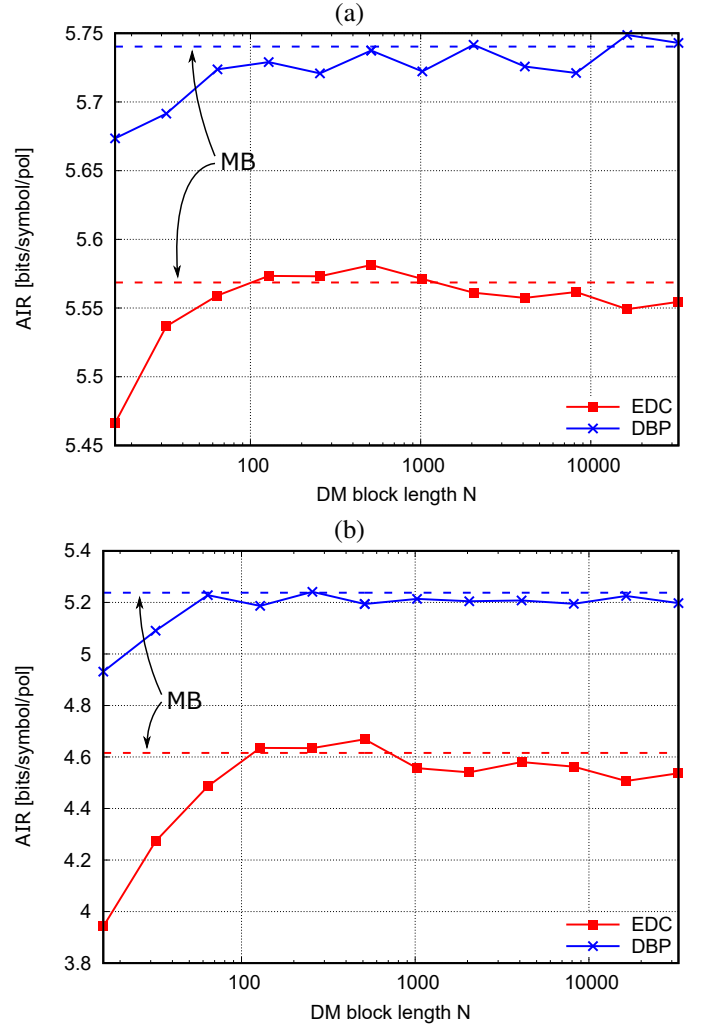


Figure 6. Maximum AIR versus DM block length using SS with $\Delta\nu = 100$ kHz laser linewidth (a) 15 spans with $N_{\text{CPR}} = 38$, (b) 27 spans with $N_{\text{CPR}} = 92$.

case using the MB distribution.

Finally, we investigated whether a similar behavior is maintained when a dispersion managed link is used. The link is made of 15 spans of 80 km SMF (parameters described in Section IV), each compensated by a 13 km span of dispersion compensating fiber (DCF) with $\alpha_{\text{dB}} = 0.57$ dB/km, $\beta_2 = 127.5$ ps²/km, and $\gamma = 6.5$ W⁻¹km⁻¹. One additional EDFA with noise figure 5 dB is added at the input of each span of DCF, to set the launch power 4 dB below that in the SMF. In this case, the optimal launch power in the SMF is 2 dBm. The block length for BPS is taken to be equal to $N_{\text{CPR}} = 800$ symbols. The system performance versus DM block length is shown in Fig. 7(b), using the SS technique and without DBP. Differently from the previous cases with the SMF, the figure shows that (i) the optimal block length for the DM is much shorter ($N = 64$ rather than $N = 256$), and (ii) a nonlinear shaping gain, of 0.15 bit/symbol/pol, is obtained in this case, even if the BPS is employed. We believe that the different behavior with respect to the previous cases is due to a twofold reason: the low SNR requires a very long BPS—which performs similar to MPR—and the negligible

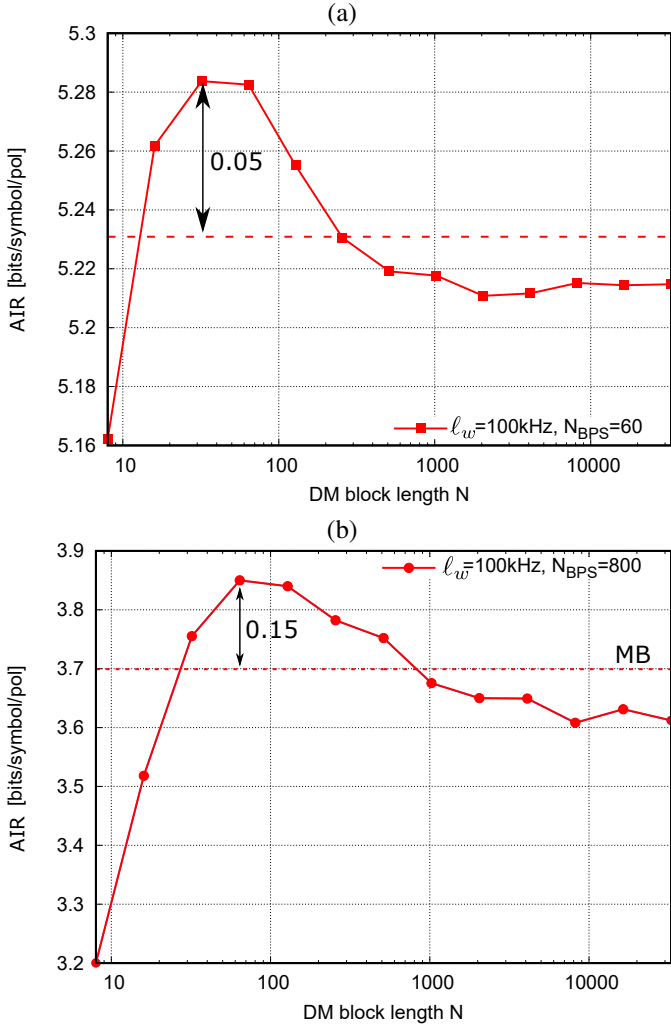


Figure 7. Maximum AIR versus DM block length using SS with $\Delta\nu = 100$ kHz laser linewidth and EDC, for a (a) 180km single span of SMF, with $N_{\text{CPR}} = 60$, (b) DCF link, with $N_{\text{CPR}} = 800$.

accumulated dispersion makes the optimal block length very short.

To better understand the interaction between nonlinear shaping gain and carrier phase recovery, Fig. 8 shows the NPN (6) obtained for the second channel of the SCOI $i = 2$, and considering the impact of the 4 channels of the SCOI, in the same setup of Fig. 4, i.e., using SS, dispersion compensation and no laser phase noise ($\Delta\nu = 0$). With reference to [43] and for the sake of simplicity, the term e_{CPR} was taken to be 0.008. The value of $2E_s/N_0$ is 20dB, corresponding to the optimum power. Firstly, let us consider the case with $N_{\text{CPR}} = 512$ in Fig. 8. This case approaches the scenario without carrier phase recovery and can be taken as a reference for the EEDI. The NPN has a minimum for SS block length $N = 32$ and then increases up to a saturation point for $N \approx 1024$. On the one hand, for very short block lengths N , the NPN increases because the SS introduces many amplitudes fluctuations, differently from the CCDM employed in [18]. On the other hand, for long block lengths N , the NPN has the same behavior shown in [18], and it is capable of predicting the system performance when carrier phase recovery is not

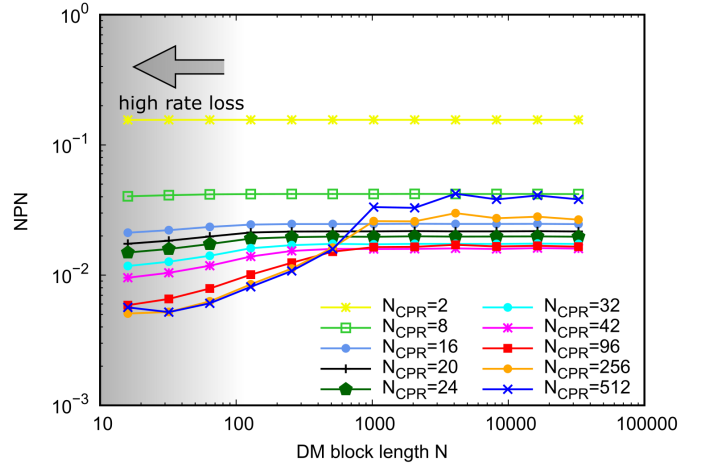


Figure 8. NPN and EEDI as a function of the DM block length, for different carrier phase recovery window

used (or one with long window is employed). Indeed, the system performance achieves a maximum value—yielding the nonlinear shaping gain—and then saturates to a lower value—corresponding to a larger NPN. Next, let us consider the cases with shorter N_{CPR} . The figure shows that (i) the NPN tends to and approaches the saturation point (for $N \rightarrow +\infty$) for shorter N , when N_{CPR} becomes smaller (ii) the saturation value achieves a minimum for $N_{\text{CPR}} = 42$, (iii) when N_{CPR} becomes smaller, the performance significantly decreases since the carrier phase recovery is not able to average out the noise and the term σ_ξ^2 becomes determining. Overall, Fig. 8 explains the interaction between carrier phase recovery and nonlinear shaping gain: a carrier phase recovery with small window (but sufficiently large to average out noise), can remove a large part of the nonlinear interference, practically hampering the nonlinear gain provided by short block length PAS—indeed, the NPN decreases until $N_{\text{CPR}} = 24$ and tends to a constant value in the DM block length N . Unfortunately, Fig. 8 cannot predict the system performance for short block lengths, since it is determined by the rate loss induced by the DM, which is not accounted for in this figure.

Finally, Figs 9(a-c) show the heat map of measured SNR, $-NPN$ and $-EEDI$, respectively, as a function of PAS block length N (x -axis) and carrier phase recovery window N_{CPR} (y -axis) in the same setup as Fig. 4 and 8. Fig 9(a), obtained through simulations, shows the SNR on the second channel of the SCOI for different DM length and CPR window. The EEDI in Fig 9(b) was evaluated with $\lambda = 0.985$, previously optimized to maximize the correlation with SNR in the case without carrier phase recovery. Comparing 9(c) and 9(b), it is evident that SNR and $-NPN$ have a similar behavior: (i) when the block length N is very short the metric achieves the best values, which unfortunately does not predict system performance since rate loss is not accounted for; (ii) the best performance is obtained when N_{CPR} is large enough to average out the noise and small enough to mitigate nonlinear interference; (iii) in the previous case the performance is almost independent on PAS block length N ; (iv) the dependence of performance on N , i.e. the nonlinear shaping gain, is evident

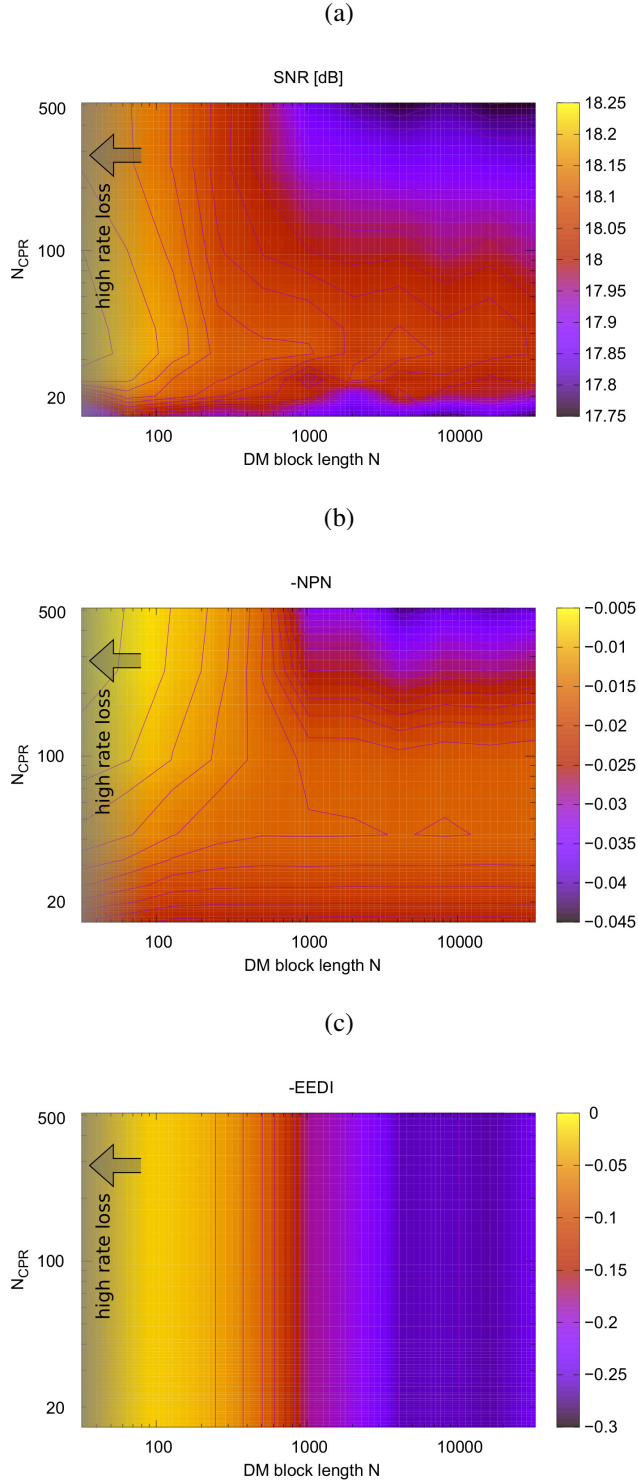


Figure 9. Heat map of (a) simulated SNR (b) $-NPN$ and (c) $-EEDI$ as a function of PAS block length N and carrier phase recovery window N_{CPR} . 15×80 km link, EDC, $\Delta\nu = 0$ kHz.

when N_{CPR} is very large and approaches MPR. Conversely, the EEDI shown in Fig 9(c) does not capture the dependence on N_{CPR} , and only show the behavior when MPR is employed. The correlation of SNR values with $-NPN$ is 0.99, while the correlation with the $-EEDI$ is 0.02

VI. CONCLUSION

This work investigated the behavior of different implementations of PAS in the nonlinear regime, considering a conventional WDM setup and different link configurations. Firstly, it was shown that, in the nonlinear regime, it is convenient to pack together the amplitudes produced by a single DM in the four symbol dimensions given by quadratures and polarizations. Next, the performance obtained using different existing DM implementations was analyzed, showing that the SS provides the best performance, not only in the linear regime, but also in the nonlinear regime. The latter result, tough counterintuitive, is a consequence of the trade-off between linear and nonlinear shaping gain. Afterwards, it was shown that, when a carrier phase recovery is included in the system, the conventional nonlinear shaping gain is negligible, not only when the BPS is optimized for inter-channel nonlinearity but also when the laser phase noise is included in the system. This behavior was exhibited for a 15×80 km SMF link, a 27×80 km SMF link, and a 1×180 km SMF link. As an exception, it was shown that, when a link with DCF is used, a significant nonlinear shaping gain of 0.15 bit/symbol/pol is obtained, also when the carrier phase recovery is included in the system. Overall, this work highlights that, despite the interesting nonlinear features of conventional DMs, (i) the nonlinear shaping gain should be properly investigated accounting for carrier phase recovery, and (ii) different shaping paradigm may be required to achieve meaningful gains in the nonlinear regime. Finally, we introduced the NPN metric, which measures the variance of the nonlinear phase noise induced in a system, taking into account different PAS block length and carrier phase recovery. The NPN metric was shown to be strongly correlated with the effective SNR of the system, and to explain the interaction of nonlinear shaping gain and carrier phase recovery.

REFERENCES

- [1] S. Civelli, E. Forestieri, and M. Secondini, "Interplay of probabilistic shaping and carrier phase recovery for nonlinearity mitigation," in *2020 European Conference on Optical Communications (ECOC)*, IEEE, 2020.
- [2] G. Böcherer, F. Steiner, and P. Schulte, "Bandwidth efficient and rate-matched low-density parity-check coded modulation," *IEEE Transactions on Communications*, vol. 63, no. 12, pp. 4651–4665, 2015.
- [3] F. Buchali, F. Steiner, G. Böcherer, L. Schmalen, P. Schulte, and W. Idler, "Rate adaptation and reach increase by probabilistically shaped 64-qam: An experimental demonstration," *Journal of Lightwave Technology*, vol. 34, no. 7, pp. 1599–1609, 2016.
- [4] T. Fehenberger, A. Alvarado, G. Böcherer, and N. Hanik, "On probabilistic shaping of quadrature amplitude modulation for the nonlinear fiber channel," *Journal of Lightwave Technology*, vol. 34, no. 21, pp. 5063–5073, 2016.
- [5] F. R. Kschischang and S. Pasupathy, "Optimal nonuniform signaling for Gaussian channels," *IEEE Transactions on Information Theory*, vol. 39, no. 3, pp. 913–929, 1993.
- [6] Y. Gültekin, W. van Houtum, and F. Willems, "On constellation shaping for short block lengths," in *2018 Symposium on Information Theory and Signal Processing in the Benelux (SITB 2018)*, pp. 86–96, University of Twente, 2018.
- [7] Y. C. Gültekin, F. M. Willems, W. J. van Houtum, and S. Şerbetli, "Approximate enumerative sphere shaping," in *2018 IEEE International Symposium on Information Theory (ISIT)*, pp. 676–680, IEEE, 2018.
- [8] Y. C. Gültekin, T. Fehenberger, A. Alvarado, and F. M. Willems, "Probabilistic shaping for finite blocklengths: Distribution matching and sphere shaping," *Entropy*, vol. 22, no. 5, p. 581, 2020.

- [9] P. Schulte and G. Böcherer, "Constant composition distribution matching," *IEEE Transactions on Information Theory*, vol. 62, no. 1, pp. 430–434, 2016.
- [10] T. Fehenberger, D. S. Millar, T. Koike-Akino, K. Kojima, and K. Parsons, "Multiset-partition distribution matching," *IEEE Transactions on Communications*, vol. 67, no. 3, pp. 1885–1893, 2018.
- [11] T. Yoshida, M. Karlsson, and E. Agrell, "Hierarchical distribution matching for probabilistically shaped coded modulation," *Journal of Lightwave Technology*, vol. 37, no. 6, pp. 1579–1589, 2019.
- [12] S. Civelli and M. Secondini, "Hierarchical distribution matching: a versatile tool for probabilistic shaping," in *Optical Fiber Communication Conference*, p. Th1G.4, Optical Society of America, 2020.
- [13] S. Civelli and M. Secondini, "Hierarchical distribution matching for probabilistic amplitude shaping," *Entropy*, vol. 22, no. 9, p. 958, 2020.
- [14] P. Nadimi Goki and L. Poti, "Rate loss reduction through look-up table design for hierarchical distribution matcher in probabilistic amplitude shaped systems," in *2021 European Conference on Optical Communication (ECOC)*, IEEE, 2021.
- [15] D. A. Mello, F. A. Barbosa, and J. D. Reis, "Interplay of probabilistic shaping and the blind phase search algorithm," *Journal of Lightwave Technology*, vol. 36, no. 22, pp. 5096–5105, 2018.
- [16] O. Geller, R. Dar, M. Feder, and M. Shtaif, "A shaping algorithm for mitigating inter-channel nonlinear phase-noise in nonlinear fiber systems," *Journal of Lightwave Technology*, vol. 34, no. 16, pp. 3884–3889, 2016.
- [17] T. Fehenberger, H. Griesser, and J.-P. Elbers, "Mitigating fiber nonlinearities by short-length probabilistic shaping," in *Optical Fiber Communication Conference*, pp. Th1I–2, Optical Society of America, 2020.
- [18] K. Wu, G. Liga, A. Sheikh, F. M. Willems, and A. Alvarado, "Temporal energy analysis of symbol sequences for fiber nonlinear interference modelling via energy dispersion index," *Journal of Lightwave Technology*, vol. 39, no. 18, pp. 5766–5782, 2021.
- [19] Y. C. Gültekin, A. Alvarado, O. Vassilieva, I. Kim, P. Palacharla, C. Okonkwo, and F. M. Willems, "On Kurtosis-limited enumerative sphere shaping for reach increase in single-span systems," in *2021 European Conference on Optical Communication (ECOC)*, IEEE, 2021.
- [20] J. Cho, X. Chen, G. Raybon, D. Che, E. Burrows, S. Olsson, and R. Tkach, "Shaping lightwaves in time and frequency for optical fiber communication," *Nature communications*, vol. 13, no. 1, pp. 1–11, 2022.
- [21] M. Secondini and E. Forestieri, "Analytical fiber-optic channel model in the presence of cross-phase modulation," *IEEE Photon. Technol. Lett.*, vol. 24, pp. 2016–2019, Nov. 2012.
- [22] R. Dar, M. Feder, A. Mecozzi, and M. Shtaif, "Properties of nonlinear noise in long, dispersion-uncompensated fiber links," *Opt. Exp.*, vol. 21, pp. 25685–25699, Nov. 2013.
- [23] R. Dar and P. J. Winzer, "Nonlinear interference mitigation: methods and potential gain," *J. Lightwave Technol.*, vol. 35, no. 4, pp. 903–930, 2017.
- [24] M. P. Yankov, T. Fehenberger, L. Barletta, and N. Hanik, "Low-complexity tracking of laser and nonlinear phase noise in WDM optical fiber systems," *J. Lightw. Technol.*, vol. 33, pp. 4975–4984, Dec. 2015.
- [25] M. Secondini, E. Agrell, E. Forestieri, D. Marsella, and M. R. Camara, "Nonlinearity mitigation in wdm systems: Models, strategies, and achievable rates," *Journal of Lightwave Technology*, vol. 37, no. 10, pp. 2270–2283, 2019.
- [26] R. Rafie Borujeny and F. Kschischang, "Why constant-composition codes reduce nonlinear interference noise," *arXiv e-prints*, p. arXiv:2203.02641, 2022.
- [27] F. Willems and J. Wuijts, "A pragmatic approach to shaped coded modulation," in *IEEE 1st Symp. on Commun. and Veh. Technol. in the Benelux*, 1993.
- [28] Y. C. Gültekin, W. J. van Houtum, A. G. Koppelaar, and F. M. Willems, "Enumerative sphere shaping for wireless communications with short packets," *IEEE Transactions on Wireless Communications*, vol. 19, no. 2, pp. 1098–1112, 2019.
- [29] Y. Chen, J. Chen, W. Li, M. Zhang, D. Liu, and M. Tang, "Squeezing out the last shaping gain with optimum enumerative sphere shaping for short block lengths," in *2021 European Conference on Optical Communication (ECOC)*, pp. 1–3, IEEE, 2021.
- [30] Y. C. Gültekin, A. Alvarado, O. Vassilieva, I. Kim, P. Palacharla, C. M. Okonkwo, and F. M. Willems, "Mitigating nonlinear interference by limiting energy variations in sphere shaping," in *Optical Fiber Communication Conference*, pp. Th3F–2, Optica Publishing Group, 2022.
- [31] P. Schulte, F. Steiner, and G. Böcherer, "shapecomm WebDM: Online constant composition distribution matcher." <http://dm.shapecomm.de>, July 2017.
- [32] A. Mecozzi and R.-J. Essiambre, "Nonlinear Shannon limit in pseudo-linear coherent systems," *J. Lightw. Technol.*, vol. 30, pp. 2011–2024, June 2012.
- [33] M. Secondini, E. Forestieri, and G. Prati, "Achievable information rate in nonlinear WDM fiber-optic systems with arbitrary modulation formats and dispersion maps," *J. Lightw. Technol.*, vol. 31, pp. 3839–3852, Dec. 2013.
- [34] A. Carena, G. Bosco, V. Curri, Y. Jiang, P. Poggiolini, and F. Forghieri, "EGN model of non-linear fiber propagation," *Opt. Exp.*, vol. 22, pp. 16335–16362, June 2014.
- [35] K. Wu, G. Liga, Y. C. Gültekin, and A. Alvarado, "Exponentially-weighted energy dispersion index for the nonlinear interference analysis of finite-blocklength shaping," in *2021 European Conference on Optical Communication (ECOC)*, IEEE, 2021.
- [36] M. Secondini and E. Forestieri, "Analytical fiber-optic channel model in the presence of cross-phase modulation," *IEEE Photonics Technology Letters*, vol. 24, no. 22, pp. 2016–2019, 2012.
- [37] M. Secondini and E. Forestieri, "On XPM mitigation in WDM fiber-optic systems," *IEEE Photon. Technol. Lett.*, vol. 26, no. 22, pp. 2252–2255, 2014.
- [38] H. Rabbani, M. Ayaz, L. Beygi, G. Liga, A. Alvarado, E. Agrell, and M. Karlsson, "Analytical modeling of nonlinear fiber propagation for four dimensional symmetric constellations," *Journal of Lightwave Technology*, vol. 39, no. 9, pp. 2704–2713, 2021.
- [39] M. Secondini, D. Marsella, and E. Forestieri, "Enhanced split-step Fourier method for digital backpropagation," in *2014 European Conference on Optical Communication (ECOC)*, pp. 1–3, IEEE, 2014.
- [40] M. Secondini, S. Rommel, G. Meloni, F. Fresi, E. Forestieri, and L. Poti, "Single-step digital backpropagation for nonlinearity mitigation," *Photon. Netw. Commun.*, vol. 31, pp. 493–502, June 2016.
- [41] S. Civelli, E. Forestieri, A. Lotsmanov, D. Razdoburdin, and M. Secondini, "Coupled-Channel Enhanced SSFM for Digital Backpropagation in WDM Systems," in *Optical Fiber Communication Conference*, Optical Society of America, 2021.
- [42] S. Civelli, E. Forestieri, A. Lotsmanov, D. Razdoburdin, and M. Secondini, "Multichannel digital backpropagation with xpm-aware essfm," in *17th International Symposium on Wireless Communication Systems (ISWCS)*, 2021.
- [43] T. Pfau, S. Hoffmann, and R. Noé, "Hardware-efficient coherent digital receiver concept with feedforward carrier recovery for m -qam constellations," *Journal of Lightwave Technology*, vol. 27, no. 8, pp. 989–999, 2009.
- [44] A. Alvarado, T. Fehenberger, B. Chen, and F. M. Willems, "Achievable information rates for fiber optics: Applications and computations," *Journal of Lightwave Technology*, vol. 36, no. 2, pp. 424–439, 2018.
- [45] E. Agrell, M. Secondini, A. Alvarado, and T. Yoshida, "Performance prediction recipes for optical links," *IEEE Photonics Technology Letters*, vol. 33, no. 18, pp. 1034–1037, 2021.
- [46] T. Fehenberger, D. S. Millar, T. Koike-Akino, K. Kojima, K. Parsons, and H. Griesser, "Analysis of nonlinear fiber interactions for finite-length constant-composition sequences," *Journal of Lightwave Technology*, vol. 38, no. 2, pp. 457–465, 2019.
- [47] W.-R. Peng, A. Li, Q. Guo, Y. Cui, and Y. Bai, "Transmission method of improved fiber nonlinearity tolerance for probabilistic amplitude shaping," *Optics Express*, vol. 28, no. 20, pp. 29430–29441, 2020.
- [48] A. Amari, S. Goossens, Y. C. Gültekin, O. Vassilieva, I. Kim, T. Ikeuchi, C. Okonkwo, F. M. Willems, and A. Alvarado, "Enumerative sphere shaping for rate adaptation and reach increase in WDM transmission systems," in *45th European Conference on Optical Communication (ECOC)*, IET, 2019.
- [49] T.-H. Nguyen, S. Mumtaz, A. Lorences-Riesgo, K. Le Trung, D. Le Gac, M. S. Neves, Y. Zhao, Y. Frignac, G. Charlet, and S. Dris, "On the performance of super-symbol PCS-QAM digital subcarrier multiplexing in coherent optical fiber systems," in *Optical Fiber Communication conference*, Optical Society of America, 2022.